BER the international journal of bridge engineering management and research

Effects of Connection on the Behavior of Bridge Deck Under Solitary Waves

Yalong Cai[1,*]; Anil K. Agrawal[2]; H.S. Tang[3]; and Ke Qu[4]

Submitted: 19 February 2025 **Accepted:** 27 March 2025 **Publication date:** 10 April 2025

DOI: 10.70465/ber.v2i2.27

Abstract: Extreme hurricanes have been causing significant damage to coastal highway bridges in the United States. To minimize the associated damage and improve the behavior of costal bridge during the extreme hurricane, this paper investigates the nonlinear interaction between water waves and superstructure of coastal bridge through a new fluid structure-interaction (FSI) model, which combines the features of ANSYS Mechanical package and Fluent software through Ansys Workbench. The paper investigates the characteristics of resultant forces of deck at the bent level to improve behavior of coastal bridge when subject to wave loads by adjusting connection properties. Four connection properties that may affect structural flexibility and four performance characteristics that are used to reflect deck behavior are selected. The Grey-based Taguchi method is then adopted to find the best combination of connection properties, which is a multi-objective, multi-factor optimization problem. After finding the optimal setting, the significance of each structure parameters is evaluated based on ANOVA analysis. Based on results from the Grey-based Taguchi method, it is concluded that the best way to improve the behavior of the bridge deck is increasing the stiffness and strength of the connection. However, with the concern that the strong connection would inevitably increase transferred wave loads and may arise localized concrete cracking problem, nonlinear SOLID element that has cracking features is adopted to model RC bridge deck. Weak region on bridge deck is identified by observing cracking patterns caused by wave loads. The efficiency of increasing reinforcement and adjusting the location to apply constraint in relieving concrete cracking problem is discussed.

Author keywords: Storm surges; Bridge decks; Uplifting; Numerical models; Gre-based Taguchi Method

Introduction

Recent extreme hurricanes accompanied by high storm surge and waves, such as Hurricane Katrina (2005), Sandy (2012), Harvey (2017), Irma (2017), Maria (2017), Ian (2022), and Helene (2024), have caused tremendous damage to coastal communities. Post-disaster surveys have revealed the vulnerability of coastal bridges, especially those with low-lying decks that were simply placed on pile caps without any constraints against uplift. For example, Fig. 1 shows the friction bearing used in the bridge carrying the U.S. 90 Route bridge over Biloxi Bay between Biloxi and Ocean Spring in Mississippi. These bearings support each end of the girders at the pier bents and provide no restraint against uplift loads. The only resistance against vertical loads is provided by gravity, which is nullified once wave loads overcome the deck weight. During Hurricane Katrina, all segments of the bridge, except those elevated above the ship channel, were unseated and shifted by wave loads. Bridges such as the one carrying the U.S. 90 Bridge over St. Louis Bay, a vital link between the communities of Pass Christian, Mississippi, and Bay St. Louis, Mississippi, had limited restraints and could not survive hurricane-induced wave loads. This type of inadequate connection design may be more common in bridges in low seismic zones, where there are no requirements for shear keys to provide lateral restraint or ties to restraint uplift movement. Considering the important role played by coastal bridges for evacuation and transportation during and after extreme events, and the possible damage to substructures caused by dislocation of superstructures or their components, it is necessary to find appropriate solutions to mitigate this mode of damage in bridges that are vulnerable to extreme hurricanes.

Since it is impractical to control wave conditions during an extreme hurricane, a retrofitting solution to enhance the performance of coastal bridges can only come from the structure itself. Even though significant efforts have been made on the prediction of accurate wave conditions and on

*Corresponding Author: Yalong Cai.
Email: yalong.cai@gmail.com
[1]STV Incorporated, Structural Engineer, 225 Park Avenue South, New York, NY 10003
[2]Professor, 160 Convent Avenue, Steinman, City College, City University of New York, New York, NY 10031
[3]Associate Professor, 160 Convent Avenue, Steinman, City College, City University of New York, New York, NY 10031
[4]Associate Professor, School of Hydraulic Engineering, Changsha University of Science and Technology, Changsha 410114, China

Discussion period open till six months from the publication date. Please submit separate discussion for each individual paper. This paper is a part of the Vol. 2 of the International Journal of Bridge Engineering, Management and Research (© BER), ISSN 3065-0569.

Figure 1. Friction bearing supporting girders in the bridge carrying U.S. 90 route over biloxi bay

the evaluation of wave loads imposed on fixed[1–7] and flexible decks,[5,7–13] research on finding an appropriate retrofitting method that could relieve damages has rarely been performed. The most direct solution generally adopted has been to elevate the bridge structure, as the common failure modes identified during post-hazard assessments have been span shifting and unseating. An elevated bridge deck is less likely to be subjected to wave loads. However, it is not practical to elevate existing bridges or to reconstruct or design a bridge as a high-rise structure because of alignment and right-of-way issues.

Many researchers have investigated drilling holes either in diaphragms or the deck to release entrapped air as a possible solution to relieving uplift forces on bridge decks.[14–17] However, this approach has several drawbacks, such as (i) drilling air-venting holes may inevitably damage the bridge structure; and (ii) the efficiency of air-venting holes decreases from a physical model to the prototype structure.[18] The air-venting holes are also less effective during rapid inundation caused by a tsunami. Hence, balancing feasibility, practicality, and efficiency, retrofitting the connection between the superstructure and substructure may have several advantages over the two potential approaches discussed previously, that is, elevating the bridge structure and drilling air-venting holes, since deck dislocation has been identified as the most common failure mode.

In recent years, several smart materials, such as shape memory alloys (SMA), have been investigated to improve performance of bridge structures during extreme events.[19] SMAs exhibit great potential in mitigating bridge unseating because of their superelasticity and significant energy-dissipation capability. Nevertheless, the application of SMAs may change the dynamic properties of the bridge structure and may create other issues related to the effects of structural flexibility on wave loads and structural responses. In the numerical study conducted by Xu and Cai,[10] increasing the structural flexibility by reducing the lateral restraining stiffness in the horizontal direction resulted in larger horizontal forces at the interface between superstructure and substructure, but such an amplification effect was not distinct on vertical forces. However, it should be noted that this study assumed very strong and stiff vertical anchorage between the superstructure and substructure. Hence, the deck had no flexibility in the vertical direction and was not allowed to elevate after the uplift wave load overcame the deck weight, although commonly used vertical anchorages do deform under wave load, as identified in the experiment by Lehrman, et al.[20]. As a result, the bridge deck could probably sway and rotate at the same time when subjected to wave loads. Since wave loads are not uniformly applied to the bridge deck and both magnitude and distribution change with time, wave loads carried by anchorages at different locations are expected to be differ. Even though the extent of movement is limited and is not likely to amplify too much with the wave load, the expected movement would inevitably change the characteristics of connection forces. The study by Lehrman, et al.[20] also showed that all anchorage types had sufficient strength to resist horizontal forces, while none of anchorage types tested exhibited sufficient strength to resist vertical loads prescribed by AASHTO[21] when wave heights exceeded 3.6m and significant trapped air was present. This means that vertical behavior and capacity are more likely to govern the failure of the connections. With the expectation of potential applications of innovative connections and the concern that either concept of updating connections will change the structural flexibility in both vertical and horizontal directions, guidance on vertical anchorage is needed to mitigate hurricane hazards on existing or new coastal bridges.

There are several questions concerning the characteristics of forces resisted by vertical anchorages. Which anchorage is subject to larger wave loads and deformations? Which structural parameters have influence on these responses? How do these structural parameters influence responses? How to evaluate the risk of vertical anchorages? Is it safe to increase horizontal flexibility? To fill these knowledge gaps, a detailed numerical study has been carried out to investigate the fluid–structure interaction (FSI) between waves and the bridge deck using commercial software packages ANSYS and FLUENT in Ansys Workbench. After validating the reliability of the numerical model, gray-based Taguchi relational analysis has been used for evaluating the behavior of vertical anchorages.

Numerical Model

Capturing the structural dynamic response under wave loads is a multi-physics problem involving fluids, structures, and their interactions, and it cannot be solved by analytical methods. Compared with significant costs and efforts required for carrying out experiments, numerical methods are much cheaper and more convenient for performing full-scale analysis. Even though it is generally accepted that the wave forces obtained from the past physical models follow the Froude Similarity law, there are still some issues with scaling up the forces from a scaled model, such as the compression of the trapped air between girders, which does not satisfy the Froude Similarity law and usually leads to a conservative value.[18] Numerical simulations can be performed by FSI in Ansys Workbench by integrating ANSYS Mechanical and Fluent (v15.0, Academic Version). ANSYS Mechanical performs structural analysis, whereas the simulation of the fluid domain is performed by Fluent. Data transfer between the coupled structure and fluid domains is performed through the Ansys Workbench platform.[22]

Structure Model

The I-10 Bridge over Escambia Bay near Pensacola, Florida, damaged during Hurricane Ivan, was adopted as the prototype bridge. The cross-section of a typical prototype bridge is shown in Fig. 2. In this bridge, all AASHTO Type III girders were simplified as beams with rectangular sections. This simplification has been commonly adopted in previous numerical studies.[1,2,10,14,15] Important geometrical properties of the bridge were: total span length, 16.64 m; width, 9.7 m; deck depth, 0.15 m; girder spacing, 1.83 m; girder width, 0.56 m; and girder height, 1.14 m. Diaphragms in the middle span of the bridge were ignored in this study.

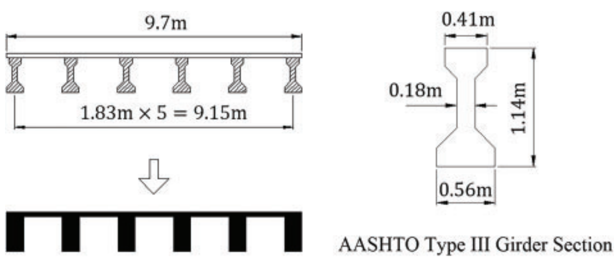

Figure 2. Geometry simplifications of the typical bridge deck section of the I–10 bridge over Escambia Bay near Pensacola, Florida.

Transient dynamic analysis was performed in ANSYS Mechanical Package to determine the dynamic response of a structure under the action of wave loads. Both rigid and deformable bridge decks were considered. The rigid bridge deck was modeled using the solid element "SOLID185." This element is defined by eight nodes, each node having three degrees of freedom (DOF). Homogeneous elastic material with high modulus of elasticity was defined for the solid elements to ensure rigid body motion of the bridge superstructure. The information about the deformable bridge deck is described in a later section. Structural flexibility was modified by changing the properties of the connection between the superstructure and substructure, which was modeled using a spring element set at the girder soffit. It should be mentioned that this study focused on structural responses at the connection level; that is, connection capability was assumed to govern the failure of the superstructure. The potential for foundation failure caused by scour or barge impact was not considered. Therefore, substructures were assumed to be fixed during the entire process of wave–bridge interaction. Since one of the objectives in this study was to differentiate the roles played by flexibilities in two directions, horizontal flexibility was treated as independent from the vertical flexibility. Flexibility in these two directions in actual bridges may be coupled.

Computational Fluid Dynamics (CFD) Model

Laminar flow was assumed to simulate the fluid domain in Fluent. Solitary wave theory was adopted to predict the wave forces on the coastal bridge. The entire computational fluid domain was divided into three zones: remeshing, fixed, and coupling zones, as shown in Fig. 3. Since the wave in this study was two-dimensional and the structural response in the third direction (the x-direction in this study) was not considered, the number of divisions in the third direction was set to one, and the bridge was expected to be subjected to the same wave conditions along this direction. The fixed zone in the simulation was created using hexahedral cells. The remeshing zone, where the coupling zone was located, was created using prism cells. Fig. 4 shows the dimensions of the remeshing zone, which was a 17.7 m × 5.79 m × 16.64 m box. The coupling zone was a bridge-shaped surface that was treated as a wall and coincided with the location of the bridge model in the structural analysis. Prism cells were used in the remeshing zone because of their advantages in adapting to complex mesh movements. Both diffusion smoothing and local remeshing methods were used to deal with the mesh updating.

The computational domain for the fluid mesh sensitivity study was 200 m in length, 15 m in height, and 16.64 m in width. The ratio of wave height to water depth (ε) was chosen as 0.08 (wave height: 0.645 m; water depth: 7.74 m). A parametric study was carried out by varying mesh sizes, dx and dy, from 0.05 to 0.2 m at the intervals of 0.05 m for time-steps (Δt) of 0.0025 and 0.005 s. Finally, a mesh resolution (dx = dy) of 0.1 m and a time step (Δt) of 0.0025 s were selected as a tradeoff between the computational cost and the accuracy of prediction.

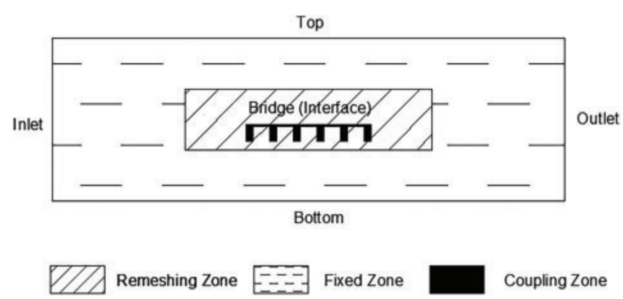

Figure 3. Schematic diagram of remeshing, fixed, and coupling zones of the computational domain

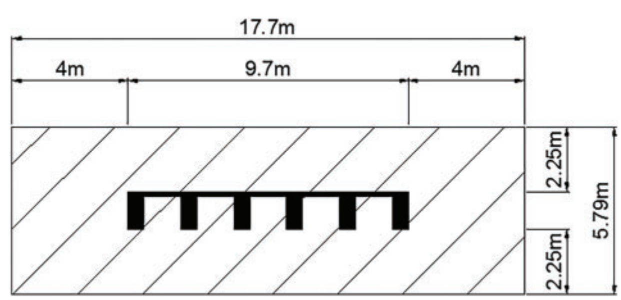

Figure 4. Dimensions of the remeshing zone

Table 1. Parameters of the 1:5 scaled model bridge for verification

	Parameter	Modal (1:5)
Geometrical properties	Girder height (m)	0.23
	Girder spacing (m)	0.37
	Deck thickness (m)	0.05
	Overall height (m)	0.28
	Span length (m)	3.32
	Span mass (kg)	1940
Flexible setup properties	Structural vibration period (s)	0.95
	Damping ratio	0
Wave conditions	Still water depth, d (m)	1.89
	Wave height, H (m)	0.5
	Wave period, T (s)	2.5
	Wavelength (m)	8.6

Validation of the Proposed Model

The capability of the model described above was verified by simulating the experimental work of Bradner et al.[8]. In this experiment, one typical span of the I-10 Bridge over Escambia Bay was built at a scale of 1:5 and was tested in a large wave flume at the Oregon State University. Table 1 presents the dimensions, weight, and flexibility of the bridge model. The superstructure was supported by two bents, which were mounted with load cells. An adjustable dynamic setup was integrated into the reaction frame to investigate the influence of structural flexibility on the loading response of the superstructure. The flexibility of the prototype bridge was achieved by installing a pair of elastic springs between the bent caps and the ends of the anchorage blocks, as shown in Fig. 5. A linear-elastic finite-element (FE) analysis was performed to identify the flexibility of the prototype substructure. The natural period of the model bridge superstructure was identified as 0.95 s, and the damping effect was neglected. Fig. 6 shows a typical wave tank condition when a series of waves were approaching the bridge specimen.

To model the experimental setup, one set of spring elements was assigned with the same horizontal stiffness of 7.1×10^3 KN/m and was attached to the bottom of each girder. In the vertical direction, since the experiment did not consider the vertical movement and connection failures, another set of springs with high vertical stiffness was placed at the ends of each girder.

In this validation test, the computational fluid domain was 40 m in length, 3.32 m in width, and 5 m in height. The mesh resolution and time steps mentioned previously were used for the numerical simulation of the test. Only one wave condition with a wave height of 0.5 m, a water depth of 1.89 m, and a wave period of 2.5 s was used.

Wave loads on the bridge superstructure were obtained by adding up the internal forces of all spring elements. Comparisons of the general characteristics of the horizontal and vertical reaction forces, as well as their comparisons with test results, are shown in Figs. 7 and 8, respectively. The plots in Fig. 7 show horizontal reaction forces for fixed and flexible setups. It is observed from Fig. 7 that the numerical simulation results match those from the experiment well in the horizontal direction for both fixed and flexible setup cases, even though the peak horizontal forces obtained from numerical simulations are smaller than those from the experiment for the fixed setup case. In the experimental results, forces imposed on the bent were also measured since load cells were mounted under the bent. These forces are not included in the numerical simulation results. The existence of the bent and a diaphragm in the middle of the span caused

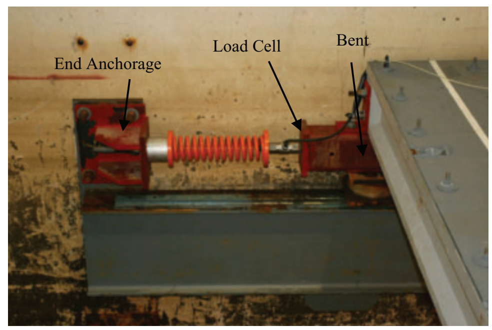

Figure 5. Soft springs with load cell installed in the model


Figure 6. Waves approaching to the bridge specimen

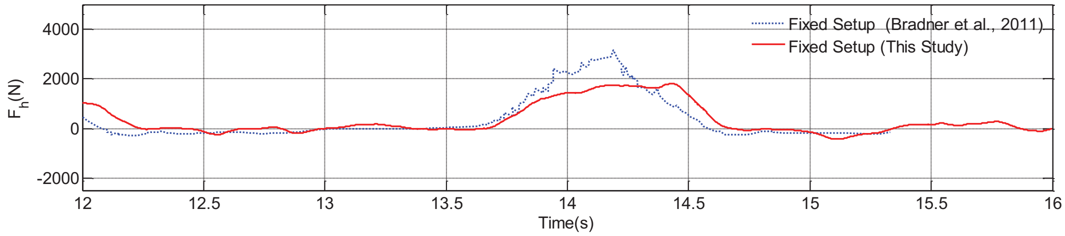

Horizontal Fixed Setup

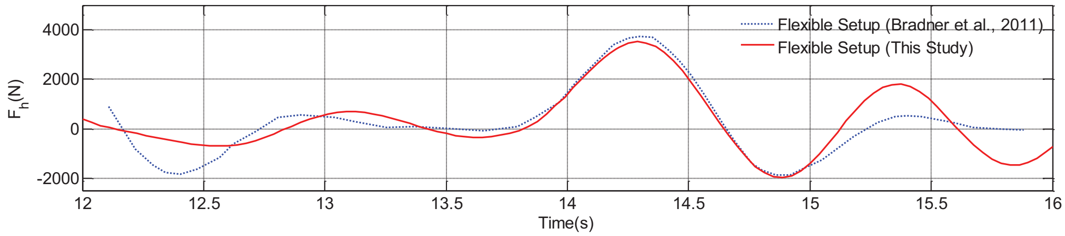

Horizontal Flexible Setup

Figure 7. Comparison of horizontal reaction forces between numerical and experimental studies

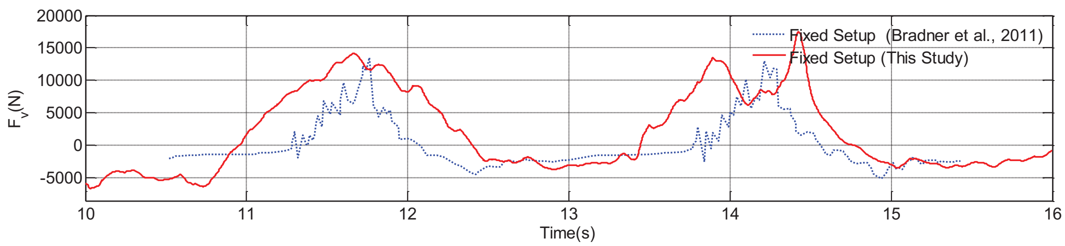

Horizontal Fixed Setup

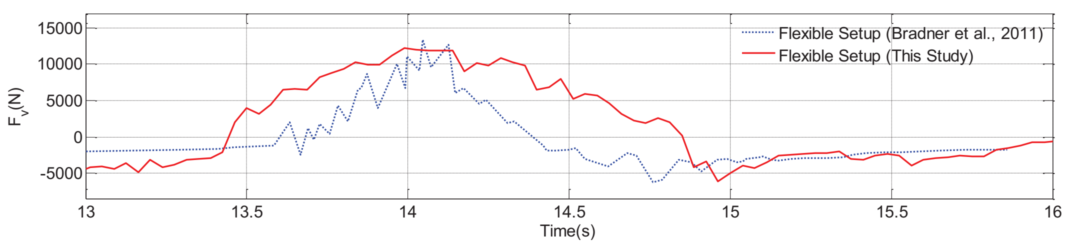

Horizontal Flexible Setup

Figure 8. Comparison of vertical reaction forces between numerical and experimental studies

some disturbance in the local fluid domain, which also might have contributed to the difference in peak horizontal forces. From the comparison of results for flexible and fixed setups in Fig. 7, it is observed that the peak value of horizontal forces for the fixed setup was 2 kN. This value was amplified to 4 kN (i.e., by a factor of 2) for the flexible setup. Fig. 8 shows vertical forces during fixed and flexible setup cases. It is observed that the amplification effect observed in the horizontal forces was not present in the vertical forces, and peak forces were between 10,000 and 15000 kN for both fixed and flexible setup cases. This is reasonable since the flexibility existed only in the horizontal direction. Both simulation and experimental results also did not show any inertia or unseating behavior. The vertical reaction force was not sensitive to fluid disturbances caused by the horizontal movement of the deck. Overall, the differences between vertical forces in Fig. 8 are very small and acceptable, considering the complexity of the phenomenon. Since numerical predictions from the proposed model follow the same trends as those observed during experiments by Bradner et al.,[8] and the difference between simulation and experimental results is possibly because of modeling simplifications, the proposed FSI model based on the laminar assumption can be considered capable of predicting reaction forces with acceptable differences in vertical forces and has been used to systematically investigate bridge–wave interaction in this research.

Verification of critical wave condition for unseating behavior

Since the unseating of a deck requires that the wave loads are large enough to overcome the deck weight, it is necessary to identify the critical wave condition that initiates the vertical movement of the deck. The significant wave height that caused the failure of the I-10 Bridge at Escambia Bay has been estimated to be 1.98 m by OEA.[23] Therefore, the critical wave condition shown in Table 2 was selected. It is noted that the prototype bridge had four head stud anchorages at two ends of each exterior girder. However, the deck was set without any vertical constraint and was placed on compression-only support to simulate considerable unseating behavior. In the horizontal direction, flexibility of $T_h = 1$ s period was set by assigning horizontal springs under each girder. This value is typical of simply supported coastal bridges. Fig. 9 illustrates the boundary conditions of the flexible bridge superstructure.

Table 2. Hazard parameters for identifying critical wave condition

Wave height (m)	Bridge elevation (m)	Water depth (m)
1.98	16.125	16.125

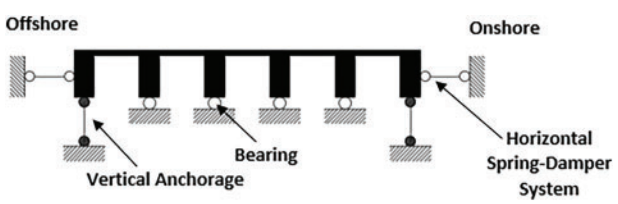

Figure 9. Boundary conditions of the deck without vertical anchorage

Fig. 10 compares the vertical load imposed on the deck with the deck weight. It is observed that the total uplift load may exceed the deck weight for certain time durations, which may cause movement of the deck. Two monitoring points under the girders on the offshore and onshore sides were selected to reflect the intensity of the overall bridge deck movement. The time history of vertical displacements at these two points is shown in Fig. 11. It is observed that displacements on both sides followed a similar pattern, while the maximum vertical displacement occurred on the onshore side under this wave condition, which is about 2 cm. Based on this observation, it is concluded that wave loads associated with the chosen hazard were strong enough to unseat the deck without any vertical constraints. In addition, since the extent of movement is much smaller than the size of the bridge, the corresponding inertia forces associated with deck movement could be ignored. This implies that all uplift loads in excess of the deck weight would have been resisted by vertical anchorages, if there had been any. As indicated before, since there were four head stud anchorages in the connection, the required tension capacity for each anchorage can be estimated as $\frac{\textit{Excess Load}}{\textit{Number of Anchorages}}$. The anchorage capacity requirement under this wave condition was 95.7 kN, which is within the identified capacity of 177.6 kN by Lehrman et al.[20]. In this sense, it is possible that the estimated critical wave height by OEA[23] is not conservative enough for the prototype bridge since the bridge had some extent of vertical constraints.

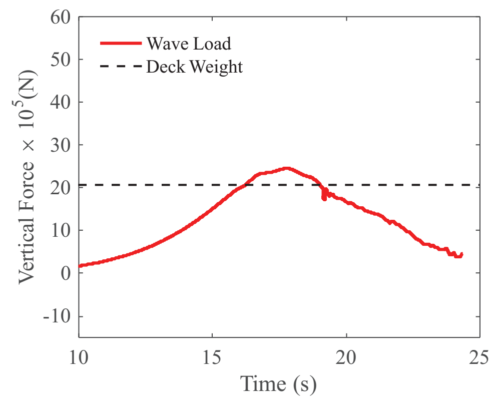

Figure 10. Comparison of vertical loads with respect to the deck weight

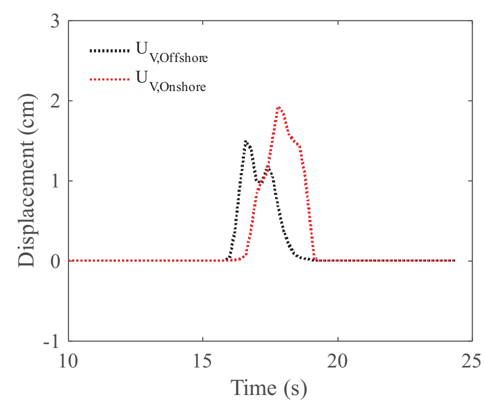

Figure 11. Time history of vertical displacement on offshore and onshore sides

The analysis of structural flexibility in the vertical direction required a simulation setup with significant vertical movements. It has been observed from previous discussion that a wave height of 1.98 m was not strong enough to initiate the vertical movement of the deck with vertical constraints. Since wave height was identified as the most significant factor influencing wave loads, a wave height of 2.58 m was chosen to test all cases for structural flexibility in the vertical direction. Similar to the simulation cases discussed previously, the girder bottom was set at the water level in this case. The testing hazard input parameters for this case are listed in Table 3.

Table 3. Testing hazard parameters

Wave height (m)	Bridge elevation (m)	Water depth (m)
2.58	16.125	16.125

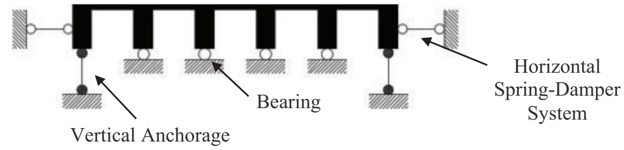

Figure 12. Boundary conditions of the deck with vertical anchorages

Gray-Based Taguchi Analysis

The Taguchi method is very popular for tackling optimization problems, especially in the field of production engineering.[24] Operating on the assumption that high-order interactions are negligible, this method uses a special set of arrays called orthogonal arrays (OA). These standard arrays stipulate the way to conduct the minimal number of experiments that can provide complete information on all factors affecting performance indices. For example, the Taguchi method is used to analyze optimal process parameters for a single quality characteristic.[25]

The Taguchi method has been applied over the last two decades for the optimization of various problems related to bridge engineering, such as in FE model updating of bridges by Sun and Yang[26] and scour reduction around spur dikes with collars by Atrodi et al.[27]. To apply this approach to a problem involving multiple objectives, weights for each quality characteristic are required. This increases uncertainty during the decision-making process. To overcome this shortcoming, the Taguchi method was integrated with gray relational analysis (GRA) to satisfy the prerequisites of optimization.

The gray system theory, proposed by Deng,[28] has proven to be useful for dealing with poor, incomplete, and uncertain information. Through GRA, a gray relational grade is obtained to evaluate the multiple performance characteristics. As a result, the optimization of the complicated multiple performance characteristics can be converted into the optimization of a single gray relational grade. Even though the gray-based Taguchi method has been used to solve problems in the manufacturing industry, such as the submerged arc welding process,[29,30] its application for bridges may have significant potential.

Determination of structural parameters

Two types of vertical springs were set to simulate the vertical anchorages and bearings in the vertical direction. Vertical anchorages have large stiffness in compression and limited tension capacities. For interior girders placed on bearings, compression-only spring elements were used. Anchorages were used only at the exterior girders in the prototype bridge, while the other girders were simply placed on pile caps without any constraints. Although anchorages may be available at every girder in bridges, this study applied anchorages only on the onshore and offshore sides. In the horizontal direction, single DOF (SDOF) spring-damper systems representing the general constraints from connection and friction were placed between the abutments and exterior girders, as illustrated in Fig. 12.

Four parameters influencing the structural response of the deck under wave loads were identified as follows: horizontal stiffness, K_H, horizontal damping, C_H, stiffness of onshore anchorage, $K_{V,on}$, and stiffness of offshore anchorage, $K_{V,off}$. To evaluate the behavior and capacity of vertical anchorages, four performance characteristics (response quantities) were selected: (i) vertical displacement at the offshore side, $D_{V,Off}$; (ii) vertical displacement at the onshore side, $D_{V,On}$; (iii) tension force in the offshore-side anchorage, $F_{V,Off}$; and (iv) tension force in the onshore-side anchorage, $F_{V,On}$. These four performance characteristics are illustrated in Fig. 13. In general, lower tension forces and deformations during the fluid–structure interaction process imply better vertical anchorage. Since structural parameters interact in a complex manner, resulting in direct or indirect influences on these four performance characteristics, an approach that can fulfill all objectives simultaneously is desired. In this sense, finding the best anchorage setting becomes a multi-objective, multi-factor optimization problem.

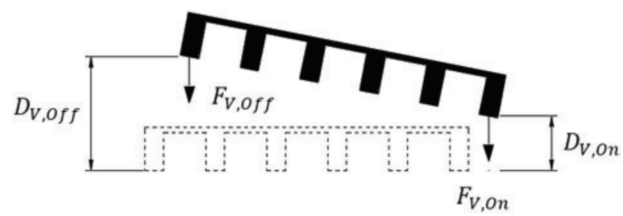

Figure 13. Schematic diagram of the performance indexes for evaluating structural performance

OA experiment

The selection of the OA is related to the total DOF of structural parameters. The DOF, N_{DOF}, defined as the number of comparisons among the structural parameters required to optimize the parameters, is calculated by

$$N_{DOF} = 1 + \sum_{i=1}^{NV} (L - 1) \tag{1}$$

In Eq. (1), NV is the number of parameters, and L is the number of levels for a parameter i. In this study, four parameters were evaluated at three different levels, as shown in Table 4. By neglecting the interaction among the structural parameters, the total DOF, as per Eq. (1), was calculated to be 9. Once the DOF was known, the next step was to select an appropriate OA. The DOF for the OA needed to be greater than or at least equal to that of the process parameters.

Table 4. Structure parameters and their levels

Structural parameters	Units	Levels		
		1	2	3
Horizontal stiffness	(KN/m)	925	1332	2081
Horizontal damping	$\left(KN.\frac{s}{m}\right)$	44.4	88.8	132.2
Offshore vertical stiffness	(KN/m)	1000	1500	2000
Onshore vertical stiffness	(KN/m)	1000	1500	2000

Table 5. Taguchi method design of cases for parameter values

Case number	K_H	C_H	$K_{V,off}$	$K_{V,on}$
1	1	1	1	1
2	1	2	2	2
3	1	3	3	3
4	2	1	2	3
5	2	2	3	1
6	2	3	1	2
7	3	1	3	2
8	3	2	1	3
9	3	3	2	1

Thereby, an L9 OA with nine rows and four columns was adopted. The resulting design matrix is shown in Table 5.[31] The maximum vertical stiffness considered in this study was close to that of existing connections.[20] However, different levels of stiffness could be introduced by modifying anchorage detailing.

Analysis and Discussion of Numerical Results

Responses based on time-history analysis of bridge–wave interaction in Ansys Workbench for the 9 cases in Table 5 were carried out. The corresponding critical values for these 9 cases in Table 5 are listed in Table 6. It is observed that, under the same wave condition, the difference between observed responses is distinct for decks with different structural properties. Moreover, all the critical vertical forces are larger than 177.6 kN (the capacity of vertical anchorage identified by Lehrman et al.[20]), which means that the existing vertical anchorage detailing was not strong enough to withstand such a wave condition. In fact, the maximum wave height that the prototype bridge experienced during Hurricane Ivan reached 3.97 m,[23] leading to the collapse of more than 3,400 feet of the bridge into the bay. It is also noted that the anchorages located on the offshore side were more likely to be subjected to larger tension forces and deformations than those on the onshore side. With an understanding of the general behavior of movable bridges, all these data were further utilized for analysis and evaluation of the preferred parameter combinations required to achieve the desired performance characteristics.

GRA

In GRA, numerical results are first normalized in the range from zero to one. This process is called gray relational generation. Following "lower the better (LB) rule", the normalized performance characteristics is expressed as

$$x_i(k) = \frac{\max y_i\,(k) - y_i\,(k)}{\max y_i\,(k) - min\ y_i\,(k)} \tag{2}$$

In Eq. (2), $x_i(k)$ is the value after the gray relational generation, $min\ y_i\,(k)$ is the smallest value of $y_i\,(k)$ for the kth response, and $max\ y_i\,(k)$ is the largest value of $y_i\,(k)$ for the kth response.

The normalized data for each performance characteristic is listed in Table 7. An ideal sequence is $x_0\,(k)$ (k = 1, 2, 3 . . . 9) for the responses, which represents the best process sequence. Next, gray relational coefficient was calculated based on normalized values using the following equations:

$$\xi_i(k) = \frac{\Delta_{min} + \psi\,\Delta_{max}}{\Delta_{0i}(k) + \psi\,\Delta_{max}} \tag{3}$$

$$\Delta_{0i}\,(k) = \|x_0\,(k) - x_i(k)\| \tag{4}$$

Table 6. Experimental results

Case number	$D_{V,Off}$(m)	$D_{V,On}$(m)	$F_{V,Off}$(N)	$F_{V,On}$(N)
1	0.2166	0.1984	216000	198400
2	0.1721	0.1543	258000	231300
3	0.1137	0.1032	227000	206000
4	0.1578	0.1085	236600	217000
5	0.1335	0.1870	267000	187000
6	0.2194	0.1319	214600	197800
7	0.1102	0.1376	220000	206000
8	0.2327	0.1091	232700	217900
9	0.1923	0.0889	288400	88900

Table 7. Data preprocessing of each response (gray relational generation)

Case number	$D_{V,Off}$	$D_{V,On}$	$F_{V,Off}$	$F_{V,On}$
Ideal sequence	1.0000	1.0000	1.0000	1.0000
1	0.1313	0.0000	0.9810	0.2310
2	0.4955	0.4027	0.4119	0.0000
3	0.9714	0.8694	0.5556	0.0344
4	0.6114	0.8210	0.7019	0.1004
5	0.8098	0.1041	0.2900	0.3111
6	0.1081	0.6073	1.0000	0.2353
7	1.0000	0.5553	0.9268	0.1777
8	0.0000	0.8155	0.7547	0.0941
9	0.3298	1.0000	0.0000	1.0000

In Eq. (3), ψ is the distinguishing coefficient with the range of $0 < \psi < 1$, Δ_{min} is the smallest value of Δ_{0i}, and Δ_{max} is the largest value of Δ_{0i}. Table 8 presents gray relational coefficients for $\psi = 0.5$. Finally, these gray relational coefficients were summed to evaluate gray relational grade by

$$\gamma_i = \frac{1}{n}\sum_{k=1}^{n} \omega_i \xi_i(k) \tag{5}$$

where n is the number of quality characteristics and ω_i is the weighting factor for the ith response.

Table 8. Gray relational coefficient of each response (with $\boldsymbol{\psi} = \mathbf{0.5}$)

Case number	$D_{V,Off}$	$D_{V,On}$	$F_{V,Off}$	$F_{V,On}$
Ideal sequence	1.0000	1.0000	1.0000	1.0000
1	0.3653	0.3333	0.9634	0.3940
2	0.4978	0.4557	0.4595	0.3333
3	0.9459	0.7929	0.5294	0.3412
4	0.5627	0.7364	0.6265	0.3573
5	0.7244	0.3582	0.4132	0.4206
6	0.3592	0.5601	1.0000	0.3953
7	1.0000	0.5292	0.8723	0.3781
8	0.3333	0.7305	0.6709	0.3556
9	0.4273	1.0000	0.3333	1.0000

As observed previously, the anchorage on the offshore side was found to be more vulnerable to wave loads. Therefore, responses on the offshore side corresponded to a larger weighting factor ($\omega_1 = \omega_3 = 0.3$), while responses on the onshore side corresponded to a lower weighting factor ($\omega_2 = \omega_4 = 0.2$). The overall performance characteristic of the multiple responses can be reflected by the calculated gray relational grades shown in Table 9. A higher value of the gray relational grade implies that the corresponding parameter combination is closer to the optimal value.

Table 9. Gray relational grade and order

Case numbers	Gray grade	Order
1	0.4811	8
2	0.4446	9
3	0.6958	2
4	0.5865	4
5	0.4915	7
6	0.5549	5
7	0.7089	1
8	0.5245	6
9	0.6948	3

For the orthogonal experimental design, it is possible to separate out the effect of each structural parameter at different levels. For example, the mean gray relational grade for the horizontal stiffness at levels 1, 2, and 3 can be calculated by averaging the gray relational grades for the experiments 1–3, 4–6, and 7–9, respectively. The mean gray relational grade ratio for each level of the other parameters can be computed in a similar manner and is shown in Table 10. In addition, the total mean of the gray relational grade for the nine cases is also calculated and listed in Table 10. The levels of the gray relational grade for different structural parameters are plotted in Fig. 14. It is observed from this figure that the optimal factor setting is $\boldsymbol{K_H(3)C_H(3)K_{V,off}(3)K_{V,on}(3)}$. The gray relational grade is highest for this setting.

Confirmation experiment

After evaluating the optimal parameter settings, the next step was to predict and verify the enhancement of performance characteristics using the optimal parametric combination. To do this, Case S1 was chosen as the initial parameter setting in which the deck was the most flexible in both directions and thus was appropriate for reflecting the behavior of the deck without any constraints.

Table 10. Response table (mean) for overall gray relational grade

Parameter	Gray relational grade						
	Level 1		Level 2		Level 3		Max.–Min.
	Cases	Grade value	Cases	Grade value	Cases	Grade value	
K_H	1, 2, 3	0.5405	4, 5, 6	0.5443	7, 8, 9	0.6427	0.1022
C_H	1, 4, 7	0.5921	2, 5, 8	0.4869	3, 6, 9	0.6485	0.1616
$K_{V,off}$	1, 6, 8	0.5201	2, 4, 9	0.5753	3, 5, 7	0.6321	0.1119
$K_{V,on}$	1, 5, 9	0.5558	2, 6, 7	0.5694	3, 4 8	0.6022	0.0464
	Total mean value of the gray relational grade = 0.5758						

The estimated gray relational grade $\hat{\gamma}$ using the optimal levels of the structural parameters can be calculated as follows:

$$\hat{\gamma} = \gamma_m + \sum_{i=1}^{o} (\overline{\gamma}_i - \gamma_m) \quad (6)$$

where γ_m is the total mean gray relational grade, $\overline{\gamma}_i$ is the mean gray relational grade at the optimal level, and o is the number of the main structural parameters that affect the responses. Eq. (6) implies that the predicted gray relational grade (optimal) is the sum of the mean gray relational grade and the summation of the difference between the overall mean gray relational grade and mean gray relational grade for each of the factors at the optimal level. Such estimation is efficient only if the individual effects of the independent structural parameters on performance parameters are separable. For example, the effect of horizontal stiffness on performance parameters does not depend on the different levels of vertical anchorage stiffness. Table 11 presents the comparison between results from the initial setting and the optimal setting. It is observed that the vertical anchorages in the optimal setting experienced much less vertical displacement and lower vertical loads, resulting in a significant improvement in the overall gray relational grade. Moreover, good agreement between the predicted and tested gray relational grades was found. Even though there was a difference between these two values (prediction and experiment under optimal process conditions), which could be caused by the interaction effects of different structural parameters, it is concluded that the main effects from individual parameters dominated the connection behavior and that potential interaction effects were limited. The role of interaction effects can be further investigated through full factorial experiments.

Analysis of variance (ANOVA)

Even though the optimal setting was determined based on a chosen wave condition, the relative importance among the structural parameters still needs to be determined so that the optimal combinations of the structural parameter levels can be determined more accurately for other wave conditions. To investigate the structural parameters significantly affecting the performance characteristics, the statistical technique called ANOVA was adopted. ANOVA separates the total variability of the response (sum of squared deviations about the grand mean) into contributions rendered by each of the parameters and the error

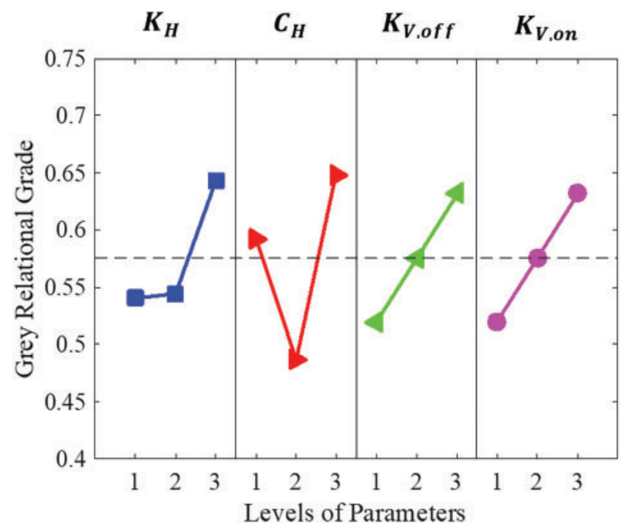

Figure 14. Gray relational grade graph

$$SS_T = SS_F + SS_e \quad (7)$$

$$SS_T = \sum_{j=1}^{p} (\gamma_j - \gamma_m)^2 \quad (8)$$

In Eqs. (7) and (8), SS_T is the total sum of squared deviations about the mean; γ_j is the mean response for the jth experiment; γ_m is the grand mean of the response; p is the number of experiments in the OA; SS_F is the sum of squared deviations due to each factor; SS_e is the sum of squared deviations due to error.

In the ANOVA table, mean square deviation is defined as

$$MS = \frac{SS\,(sum\ of\ squared\ deviation)}{DF\,(degree\ of\ freedom)} \quad (9)$$

The mean square deviation of a particular structural parameter indicates whether the performance objective, the gray relational grade in this case, is sensitive to the changes in level settings. If the sum of squared deviations is close to zero or insignificant, it could imply that the design variables are not influencing the performance of the process. Table 12 summarizes the mean square deviations of each parameter.

Table 11. Results of confirmation experiment

	Initial parameter setting	Optimal process condition	
		Prediction	Experiment
Level of parameters	$K_H(1)C_H(1)K_{V,off}(1)K_{V,on}(1)$.	$K_H(3)C_H(3)K_{V,off}(3)K_{V,on}(3)$.	$K_H(3)C_H(3)K_{V,off}(3)K_{V,on}(3)$.
$D_{V,Off}$(m)	0.2166		0.1113
$D_{V,On}$(m)	0.1984		0.1022
$F_{V,Off}$(KN)	216000		222000
$F_{V,ON}$(KN)	198400		204000
Gray relational grade	0.4811	0.7981	0.7791
Improvement in gray relational grade = 0.2980			

Table 12. Mean square deviation of each parameter

	SS	DF	MS
K_H	0.0202	2	0.0101
C_H	0.0404	2	0.0202
$K_{V,off}$	0.0188	2	0.0094
$K_{V,on}$	0.0034	2	0.0017

Table 13. ANOVA analysis based on adjusted MS

	Adjusted MS	F	P
K_H	0.0101	5.94	0.144
C_H	0.0202	11.88	0.077
$K_{V,off}$	0.0094	5.53	0.153
$K_{V,on}$	0.0000	0.00	0
Error		0.0017	

It is evident that horizontal damping was the most significant factor, while the vertical stiffness of anchorage on the onshore side was the least significant factor. Hence, by setting vertical anchorage on the onshore side as noise, the variance of noise was calculated to be 0.0017. The P-value (probability of significance) was calculated based on the F-value, which is defined as

$$F = \frac{MS\ for\ individual\ parameter}{MS\ for\ error} \tag{10}$$

If the P-value for a term appeared is less than 0.05 (95% confidence level), then the effect of that parameter is considered significant on the selected response. ANOVA based on adjusted mean square for the overall gray relational grade is shown in Table 13. It is noted that the minimum P-value, which corresponds to horizontal damping, is still larger than 0.05. Hence, the efficiency of modifying flexibility to prevent connection failure is limited, although damping seems to play a more significant role than other parameters. Compared to wave conditions, which are uncontrollable, updating connections between the superstructure and substructure is expected to be more effective, and the influence of structural parameters may probably be sensitive to wave conditions. To control and relieve forces taken by the connection, stiff anchorage detailing is recommended.

Cracking associated with strengthening connection

It is noted from the previous discussion that the best approach to improving the behavior of the bridge deck is by increasing the stiffness and strength of the connection. Hence, the ideal connection may need to be very stiff and strong enough to carry all wave loads. Constrained by such connections, the bridge deck will remain almost static when subjected to wave loads, which may cause the connections to bear more wave loads. Conversely, a weak connection may fail before the wave load reaches its maximum value. In this case, the load transferred to the substructure may be limited due to the bridge deck swaying away. On the contrary, a strong connection would transfer all wave loads to the substructure, which may compromise the stability and safety of the substructure. Furthermore, as more load is imposed on the bridge deck, it may experience stress concentration and large deformation, which may cause localized concrete cracking in the deck.

To simulate such nonlinear behavior, the bridge deck was modeled as a deformable body in LS-DYNA, as shown in Fig. 15. The reinforced concrete in the deck was represented using an eight-node SOLID65 element. This element accommodates up to four different materials within each element. For reinforced concrete, these materials include one matrix material (concrete) and three reinforcing materials (steel). In this study, only one reinforcing material was utilized. The material properties for the deck are provided in Table 14.

The reinforcement is assumed to have only uniaxial stiffness and behaves elastically. Instead of being modeled separately, the reinforcement is assumed to be smeared throughout the element. In the smeared model, the concrete and reinforcement mesh share the same nodes, meaning the region occupied by concrete is also occupied by reinforcement. When the major principal stress reaches the tensile strength, which is 3 MPa in this study, a crack is initiated. The nucleation of one or more cracks within the volume attributed to an integration point results in a deterioration of the current stiffness and strength at that integration point. We do not consider the relaxation of any tensile stress in the deck. When a crack occurs during the analysis, the stress available at that node drops to zero.

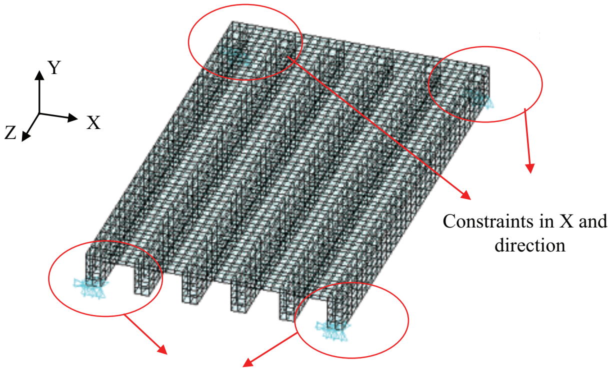

Figure 15. Boundary conditions of the deck with connections available under exterior girders

Table 14. Mechanical properties of materials

Mechanical properties	Concrete	Steel
Compressive strength (MPa)	60	–
Tensile strength (MPa)	3	–
Modulus of elasticity (GPa)	30	210
Poisson ratio	0.2	0.3
Density (kg/m^3)	2400	7800

The reinforcement detailing is represented by the volume ratio and orientation angle. The volume ratio of reinforcement is assumed to be 2% in x, y, and z directions. The crushing capacity of concrete elements is turned off to avoid convergence problems. However, the compressive strength of concrete is assumed to be 60 MPa.

When subjected to wave loading, upward wave loads exceeding the deck weight are carried by anchorages. In the prototype bridge, anchorages are only available at the exterior girders. Therefore, constraints are applied along the bottom edge of these exterior girders, assuming that the constrained edges are completely fixed. Since the interior girders have no capacity to resist tension forces, they are expected to detach from the substructure and deform freely once wave loads overcome the deck weight. As the bridge deck is simply supported, one end of the deck is not constrained in the Z direction, as previously illustrated in Fig. 13.

As no deck flexibility is expected, static analysis was performed to simulate cracking. Wave loads imposed on the static bridge-shaped wall were first obtained using the FLUENT environment and were extracted for application to the structural model of the bridge in LS-DYNA. The testing wave condition was chosen with a wave height of 2.58 m. The deck bottom was set at the water level. To observe the process of crack propagation after the wave load exceeded the deck weight, wave loads at typical instants were selected to interact with the bridge deck. Fig. 16 shows the distribution of wave loads at a time instant of t = 15.4 s, when $F_V = F_{V,max} = 2791$ kN and $F_H = 198$ kN. It is noted that the wave loads were not uniformly distributed on the bridge deck. At this moment, the offshore side was subjected to larger water pressure forces. In the LS-DYNA model of the deck, the effect of gravity effect was simulated by assigning an upward acceleration. Both gravity and wave loads were applied in the first substep and remained constant for all subsequent load steps.

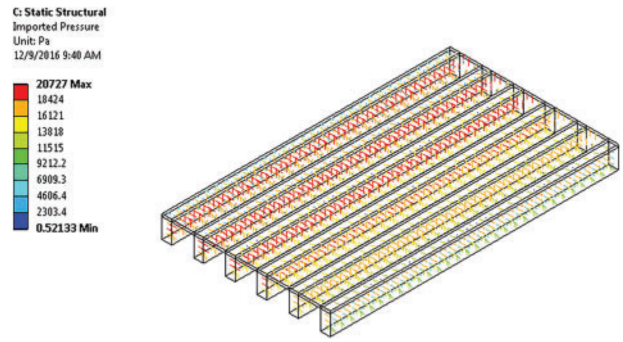

Figure 16. Imported pressure forces on bridge deck (T = 15.4 s)

Fig. 17 illustrates the cracking process of the deck with exterior girders constrained. The FE model shows that a few cracks first appeared near the end of the exterior girder on the offshore side at 14.2 seconds, specifically at the intersection between the girder and slab. As the loads increased, cracks developed at the other end of the exterior girder on the offshore side, and these initial cracks began to propagate toward mid-span. The major principal stress close to the constrained edge reached the tensile strength and a few cracks developed at this location too. At t = 14.8 seconds, major cracks on the offshore side continued to extend toward the middle part of the girder span, while cracks started to appear on the onshore side. Similar to the offshore side, cracks were initiated and concentrated in the region between the slab and exterior girder on the onshore side. The vertical wave load reached its maximum value at t = 15.4 sec. By this time, major cracks had extended to approximately one-third of the girder span. It should be noted that the prestressed tendons in the prototype bridge were not modeled, and the assigned reinforcement was an idealized representation of the actual reinforcement details. All simulations were performed after the deck weight was counterbalanced by its self-weight. The observed cracks in the generally reinforced deck were sufficient to identify weak regions that require special strengthening.

The results presented in Fig. 17 suggest that strengthening connections alone cannot completely protect the bridge deck from wave-induced damages. A fully restrained deck may still sustain damage or even fail due to localized concrete cracking.

Although the proposed approach has limitations, namely local fracture and crack width cannot be predicted accurately, the simulation results demonstrate potential cracking

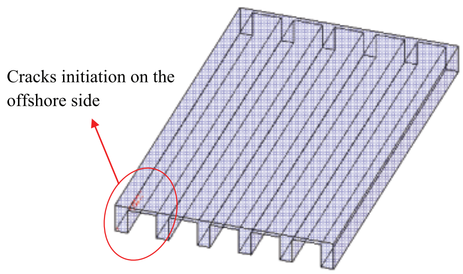

t=14.2s, $F_H = 138KN$, $F_V = 2253KN$

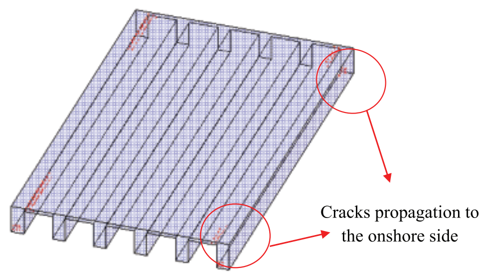

t=14.8s, $F_H = 165KN$, $F_V = 2597KN$

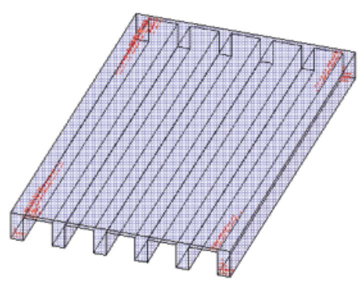

t=15.4s, $F_H = 198KN$, $F_V = 2791KN$

Figure 17. Crack propagation in the bridge deck subjected to wave loads

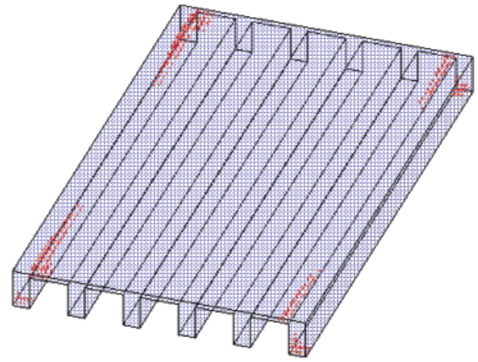

(b) Volume ratio=2%

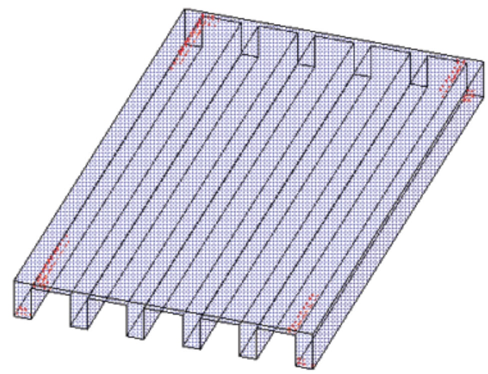

(c) Volume ratio=3%

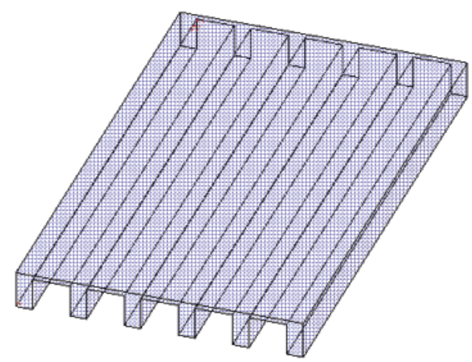

(d) Volume ratio=4%

Figure 18. Cracking pattern of decks with different reinforcement volume ratios

patterns and provide preliminary results on the region of the deck requiring strengthening. Since the wave loads are not uniformly distributed on the bridge deck, and the offshore side is subject to larger water pressure forces when $F_V = F_{V,max}$, the offshore side, especially the region close to constraints, is more likely to undergo cracking.

Current design approaches to controlling concrete cracking focus on limiting the spacing of reinforcement. In the FE model, this is achieved by adjusting the reinforcement volume ratio. To investigate the effectiveness of adding reinforcement to control crack development, decks with different reinforcement volume ratios (2%, 3%, and 4%) were simulated under the same wave loading. Fig. 18 shows the results for the situation where $F_V = F_{V,max}$. It is observed that the number of cracks generally decreases as the reinforcement volume increases. Most cracks observed in Fig. 18a disappear in Fig. 18d, which corresponds to a reinforcement volume ratio of 4%.

In addition to improving the tensile strength of the deck by adding reinforcement, another approach to crack control is adjusting the load distribution to relieve stress concentration in the deck. When all girders have vertical anchorages, the loads carried by the anchorages decrease significantly, resulting in better crack control. However, when the number of anchorages is limited, for example, two pairs of anchorages, the arrangement of anchorages may play an important role in load distribution. To investigate the effect of different anchorage locations, apart from anchorages at exterior girders, two other anchorage arrangements were considered

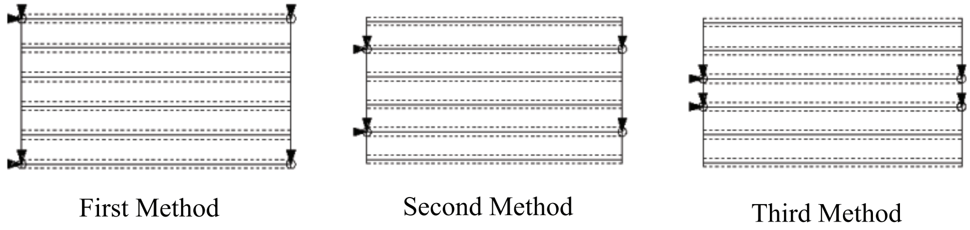

Figure 19. Sketch of three methods of implementing anchorages

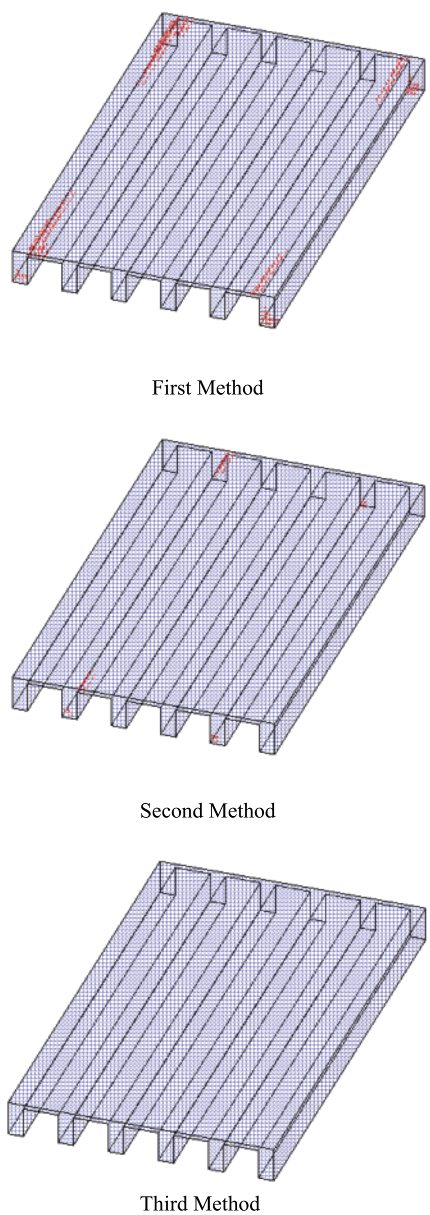

Figure 20. Cracking pattern of decks with three scenarios of deck anchorages

for comparison. In the second method, two interior girders adjacent to the exterior girders are also secured by anchorages. In the third method, two interior girders located in the middle are secured by anchorages. The reinforcement volume ratio is set at 2% for all three cases. These three anchorage arrangements are shown in Fig. 19. The wave conditions remain the same as before, with a wave height of 2.58 m and the bottom of the bridge deck positioned at the water level.

Fig. 20 shows the results of the simulation. By comparing the crack patterns for the three cases, it is observed that the deck in the 3rd case does not have any cracks. Hence, by moving the anchorages from exterior to interior girders, it is possible to protect the bridge deck against localized concrete cracking compared to when anchorages are positioned at exterior girders. Consequently, during the design of anchorages for bridge decks subjected to wave loads, cracking in the deck can be minimized by evaluating different anchorage arrangements for girders.

Conclusions

A new approach for evaluating the reliability of connections in coastal bridges subjected to wave loads during hurricanes is investigated in this research. Four common controllable structural parameters that influence structural flexibility have been selected and discussed. This is the first study to explore the combination of the Taguchi method and GRA to determine the optimal combination of structural parameters for bridges. Appropriate assumptions were made to convert multiple structural responses into a gray relational grade to find an optimal combination of structural parameters. Although the influence of structural parameters varies with wave conditions, the optimal combination of structural parameters indicates that stiffer connections perform better in terms of the safety and stability of the entire bridge deck. Conversely, a deck with flexible connections is at a higher risk of failure. However, stiff anchorage of girders may cause significant stress concentration and cracking in the deck, which can be relieved by optimizing the reinforcement volume ratio and the locations of girder anchorages. Simulation results show that anchorages placed at interior girders are less likely to cause stress concentration and cracking in the deck. However, large transferred loads may contribute to foundation failure, which can be prevented by limiting the magnitude of transferred loads through highly stiff but brittle anchorage detailing. This issue should be investigated in future studies.

References

[1] Huang W, Xiao H. Numerical modeling of dynamic wave force acting on Escambia Bay Bridge deck during Hurricane Ivan. *J Waterway, Port, Coast, Ocean Eng*. 2009;135(4): 164–175. doi:10.1061/(ASCE)0733-950X(2009)135:.

[2] Jin J, Meng B. Computation of wave loads on the superstructures of coastal highway bridges. *Ocean Eng*. 2011; 38(17–18):2185–2200. doi:10.1016/j.oceaneng.2011.09.029.

[3] Xu G, Cai CS. Wave forces on biloxi bay bridge decks with inclinations under solitary waves. *J Perform Constr Facil*. 2015;29(6):04014150. doi:10.1061/(ASCE)CF.1943-5509.0000644.

[4] Xu G, Cai CS, Deng L. Numerical prediction of solitary wave forces on a typical coastal bridge deck with girders. *Struct Infrastruct Eng*. 2016;13(2):254–272. doi:10.1080/15732479.2016.1158195.

[5] Cai Y, Agrawal A, Qu K, Tang HS. Numerical investigation of connection forces of a coastal bridge deck impacted by solitary waves. *J Bridge Eng*. 2018;23(1):04017108. doi:10.1061/(ASCE)BE.1943-5592.0001135.

[6] Huang B, Hou J, Yang Z, Zhou J, Ren Q, Zhu B. Influences of the pile-restrained floating breakwater on extreme wave forces of coastal bridge with box-girder superstructure under the action of two-dimensional focused waves. *Appl Ocean Res*. 2023;134(2):103508. doi:10.1016/j.apor.2023.103508.

[7] Huang B, Chen P, Yang Z, Zhou J, Ren Q, Zhu B. Experimental study of dynamic response of the box-girder coastal bridge under the regular wave actions with considering the wave-structure coupling. *Appl Ocean Res*. 2024;150(9):104112. doi:10.1016/j.apor.2024.104112.

[8] Bradner C, Schumacher T, Cox D, Higgins C. Experimental setup for a large-scale bridge superstructure model subjected to waves. *J Waterw, Port, Coast Ocean Eng*. 2011;137(1):3–11. doi:10.1061/(ASCE)WW.1943-5460.0000059.

[9] Ataei N, Padgett JE. Influential fluid-structure interaction modelling parameters on the response of bridges vulnerable to coastal storms. *Struct Infrastruct Eng*. 2015;11(3):321–33. doi:10.1080/15732479.2013.879602.

[10] Xu G, Cai CS. Numerical simulations of lateral restraining stiffness effect on bridge deck-wave interaction under solitary waves. *Eng Struct*. 2015;101(2):337–351. doi:10.1016/j.engstruct.2015.07.031.

[11] Chen XB, Zhan JM, Chen Q, Cox D. Numerical modeling of wave forces on movable bridge decks. *J Bridge Eng*. 2016; 21(9):04016055. doi:10.1061/(ASCE)BE.1943-5592.0000922.

[12] Istrati D. *Large-Scale Experiments of Tsunami Inundation of Bridges Including Fluid-Structure-Interaction*. Dissertation. University of Nevada, Reno; 2017.

[13] Yuan P, Zhu D, Dong Y, Xu G. Response-based bridge deck limit state considering component-level failure under extreme wave. *Mar Struct*. 2022;83(1):103184. doi:10.1016/j.marstruc.2022.103184.

[14] Bozorgnia M, Lee J-J, Raichlen F. Wave structure interaction: role of trapped air on wave impact and uplift forces. *Coast Eng Proc*. 2011;1(32):57. doi:10.9753/icce.v32.structures.57.

[15] Hayatdavoodi M, Seiffert B, Ertekin RC. Experiments and computations of solitary-wave forces on a coastal-bridge deck. Part II: deck with girders. *Coast Eng*. 2014;88:210–228. doi:10.1016/j.coastaleng.2014.02.007.

[16] Seiffert B, Hayatdavoodi M, Ertekin RC. Experiments and computations of solitary-wave forces on a coastal-bridge deck. *Part I: Flat Plate, Coast Eng*. 2014;88:194–209. doi:10.1016/j.coastaleng.2014.01.005.

[17] Liu Z, Liu J, Guo A. Load characteristics of coastal bridge deck with air vents under wind and waves combined action. *Appl Ocean Res*. 2023;130:103441.

[18] Cuomo G, Shimosako K, Takahashi S. Wave-in-deck loads on coastal bridges and the role of air. *Coast Eng*. 2009;56(8):793–809. doi:10.1016/j.coastaleng.2009.01.005.

[19] Dong J, Cai C, Okeil A. Overview of potential and existing applications of shape memory alloys in bridges. *J Bridge Eng ASCE*. 2011;16(2):305–315. doi:10.1061/(ASCE)BE.1943-5592.0000145.

[20] Lehrman JB, Higgins C, Cox D. Performance of highway bridge girder anchorages under simulated hurricane wave induced loads. *J Bridge Eng*. 2012;17(2):259–271. doi:10.1061/(ASCE)BE.1943-5592.0000262.

[21] AASHTO. *AASHTO Guide Specifications for Bridges Vulnerable to Coastal Storms*. Washington, D.C: American Association of State Highway Transportation Officials; 2008.

[22] Chimakurthi SK, Reuss S, Tooley M, Scampoli S. ANSYS workbench system coupling: a state-of-the-art computational framework for analyzing multiphysics problems. *Eng Comput*. 2018;34(2):385–411. doi:10.1007/s00366-017-0548-4.

[23] OEA. *Ocean Engineering Associates Inc., Hurricane Impact Analysis and Development of Design Criteria for the I- 10 Bridges Over Escambia Bay*. Gainesville, FL: Ocean Engineering Associates, Inc; 2005.

[24] Yang WH, Tarng YS. Design optimization of cutting parameters for turing operations based on the Taguchi method. *J Mater Process Technol*. 1998;84(1–3):122–129. doi:10.1016/S0924-0136(98)00079-X.

[25] Lin CL. Use of the taguchi method and grey relational analysis to optimize turning operations with multiple performance characteristics. *Mater Manuf Process*. 2004;19(2):209–220. doi:10.1081/AMP-120029852.

[26] Sun H, Yang L. An improved Taguchi method and its application in finite element model updating of bridges. *Key Eng Mater*. 2011;456:51–65. doi:10.4028/www.scientific.net/KEM.456.51.

[27] Atarodi A, Karami H, Ardeshir A, Hosseini K, Lampert D. Experimental investigation of scour reduction around spur dikes by collar using Taguchi method. *Iran J Sci Technol, Trans Civi Eng*. 2021;45:971–983.

[28] Deng J. Control problems of grey systems. *Syst Contr Lett*. 1982;5:288–294.

[29] Tarng YS, Juang SC, Chang CH. The use of grey-based Taguchi methods to determine submerged arc welding process parameters in hardfacing. *J Mater Process Technol*. 2002;128(1–3):1–6. doi:10.1016/S0924-0136(01)01261-4.

[30] Datta S, Bandyopadhyay A, Pal PK. Grey-based Taguchi method for optimization of bead geometry in submerged arc bead-on-plate welding. *Int J Adv Manuf Technol*. 2008;39(11–12):1136–1143. doi:10.1007/s00170-007-1283-6.

[31] Kacker RN, Lagergren ES, Filliben JJ. Taguchi's orthogonal arrays are classical designs of experiments. *J Res Nat Inst Stand Technol*. 1991;96(5):577. doi:10.6028/jres.096.034.